JOURNAL OF GEOPHYSICAL RESEARCH, VOL. 96, NO. D10, PAGES 18,735–18,752, OCTOBER 20, 1991

AIRBORNE MEASUREMENTS OF PARTICLE AND GAS EMISSIONS FROM THE 1990 VOLCANIC ERUPTIONS OF MOUNT REDOUBT

Peter V. Hobbs, Lawrence F. Radke,[1] Jamie H. Lyons, Ronald J. Ferek, and Derek J. Coffman

Department of Atmospheric Sciences, University of Washington, Seattle

Thomas J. Casadevall

U.S. Geological Survey, Denver

Abstract. Airborne in situ and remote sensing (lidar and correlation spectrometer) measurements are described for the volcanic emissions from Mount Redoubt, Alaska, in January and June 1990. The lidar provided excellent real-time information on the distribution of the volcanic effluents. In postanalysis the lidar observations were used to determine cross-sectional areas of the plumes of emissions which, together with the airborne in situ measurements, were used to derive the fluxes of particles and gases from the volcano. For the intraeruptive emissions the ranges of the derived fluxes were for water vapor, ~160–9440 kg s^{-1}; for CO_2, ~30–1710 kg s^{-1}; for SO_2, ~1–140 kg s^{-1}; for particles (<48 μm diameter), ~1–6 kg s^{-1}; for $SO_4^=$, <0.1–2 kg s^{-1}; for HCl, <0.01–2 kg s^{-1}; and for NO_x, <0.1–2 kg s^{-1}. Independent measurements of SO_2 from a correlation spectrometer during the period of active dome growth between late March and early June 1990 gave fluxes from 12 to 75 kg s^{-1}. The particles in the intraeruptive emissions consisted primarily of silicate rock and mineral fragments devoid of any sulfuric acid coating. Very little of the SO_2 (~0.1%) was oxidized to sulfate in the cold, dark conditions of the Arctic atmosphere. During a large eruption of Mount Redoubt on January 8, 1990, the particle (<48 μm diameter) emission flux averaged ~10^4 kg s^{-1}. During posteruptive emissions on June 11, 1990, the fluxes of both particles and gases were either close to or less than our lower detection limits (except for water vapor, which had a flux of ~6 x 10^3 kg s^{-1}).

Introduction

On December 14, 1989, after 21 years of quiescence the Redoubt Volcano, located 180 km southwest of Anchorage, Alaska, erupted violently, sending an ash cloud to a peak altitude of over 12 km. This eruption was the seventh eruptive sequence since Captain James Cook named the volcano in 1798. On December 15, 1989, the four turbofan engines of a new Boeing 747-400 aircraft stalled when it encountered the ash cloud while descending for a landing at Anchorage. The aircraft fell for about 8 min, losing more than 3 km of altitude, before the crew restarted two of the engines. Subsequently, the other two engines were started, and the aircraft landed safely. However, $80 million of damage was done to the nearly new aircraft. On the same day, two other aircraft were damaged by encounters with the ash cloud. During the next month or so, air traffic in Anchorage area was severely disrupted by the emissions from Mount Redoubt.

Following requests from the Federal Aviation Administration (FAA), the National Oceanic and Atmospheric Administration (NOAA), and Senator Ted Steven's staff in Alaska, our research group deployed its Convair C-131A research aircraft to Anchorage on January 3, 1990, for the purpose of studying the emissions from Redoubt. This airborne research facility has been used to study the emissions from many volcanoes, including Mount Baker, Washington [Radke et al., 1976], St. Augustine, Alaska [Hobbs et al., 1977], Mount Mageik and Mount Martin [Stith et al., 1978], and Mount St. Helens [Hobbs et al., 1981, 1982]. Descriptions of the instrumentation and techniques that we use for obtaining airborne in situ measurements of volcanic emissions may be found in these papers.

The principal goals of our studies of Mount Redoubt were to characterize the physical and chemical nature of the volcanic emissions, to test the suitability of a new airborne lidar system aboard the Convair C-131A for remotely detecting clouds and plumes of volcanic ash, and to use a combination of in situ and remote sensing measurements to obtain estimates of the fluxes of various gases and particles from the volcano.

Volcanic Activity

After a series of vent-clearing eruptions of Mount Redoubt (peak elevation 3.08 km mean sea level (msl)) on December 14 and 15, 1989, the volcano entered a phase of dome building that lasted until January 2, 1990, when the paroxysmal eruption in the 1989-1990 sequence destroyed more than 80% of the new dome [Alaska Volcano Observatory Staff, 1990; Brantley, 1990]. During the first period of our airborne measurements, from January 4–12, 1990, Mount Redoubt largely vented steam and small amounts of ash, which produced a plume that could generally be seen to extend more than 100 km downwind. On January 4 there was vigorous steaming, with the top of the plume reaching to ~4.6 km above msl. The emissions were less vigorous on the morning of January 5, but by the middle of the afternoon the activity was punctuated by steam explosions and an increase in ash emissions. On January 6 a comparatively large steam explosion occurred, which reached a height of ~6 km msl. This was followed by minor explosions and venting. On January 8 there was another major volcanic eruption that destroyed the remainder of the dome. Ash was carried to more than 10 km msl, and about 1 cm of ash was deposited in Kenai which is located about 80 km NE of Mount Redoubt. By the afternoon of January 8 the volcanic activity looked much the same as it did on January 4, except that the plume was more opaque. The volcano continued to vent steam and, to a lesser extent, ash

[1]Now at NCAR, Research Aviation Facility, Boulder, Colorado.

Paper number 91JD01635.
0148-0227/91/91JD-01635$5.00

Another explosion of steam occurred on January 11. We sampled these emissions, but our operations were hampered by snow and cloud. The following day (January 12) the volcanic plume was not obscured by clouds, and it was sampled at 3.3 km msl.

On June 11, 1990, we sampled the effluents from Mount Redoubt at 1 to 2 km msl under partly cloudy conditions. This period of sampling coincided with the end of observable growth of the Mount Redoubt lava dome [Brantley, 1990] with the volcano markedly less active than during our January measurements.

With the exception of the measurements that we obtained just after midday on our first flight on January 8, we will refer to all of the measurements obtained in January as being intraeruptive emissions. After our last measurements on January 12, another major eruption occurred on January 16, and Mount Redoubt continued to erupt periodically through April 1990. The last eruption was on April 26, 1990. This was followed by slow growth of the lava dome until early June. We will refer to the measurements that we obtained on June 11, 1990, as being in posteruptive emissions.

Instrumentation and Sampling Strategy

The Convair C-131A research aircraft was equipped with in situ samplers for measuring continuously the concentrations and size distributions of airborne particles in the size range 0.05–4500 μm, the concentrations of SO_2, NO, NO_2, CO, CO_2, and O_3, and for measuring (with the aid of chemically treated filters) the concentrations of $SO_4^=$ and HCl (and in June H_2S) in the air. Also aboard the aircraft was a recently built dual wavelength Nd-YAG laser lidar. The lidar was mounted within the aircraft fuselage and pointed directly upward through a window. The receiver was a 33.6 cm Cassegrainian telescope with a photomultiplier tube detector at 0.532 μm and an avalanche photodiode detector at 1.064 μm. The lidar was operated at a vertical resolution of 4 m and a horizontal resolution of 8 m. Previous airborne lidar measurements of volcanic clouds were in quiescent plumes containing little or no solid silicate ash particles [Casadevall et al., 1984]. One of the principal goals of our study of the volcanic emissions from Mount Redoubt was to investigate how well this lidar could detect volcanic ash particles.

A correlation spectrometer (Model COSPEC IV, Barringer Research, Toronto) belonging to the Alaska Volcano Observatory has been used regularly to measure sulfur dioxide emission rates at Mount Redoubt since March 1990. This same instrument was operated aboard the University of Washington's Convair research aircraft on June 11, 1990, simultaneously with lidar and in situ sampling methods. Using near-UV radiation from the Sun as a source, the column density of SO_2 is measured remotely by comparing spectral absorption by SO_2 with spectral regions where absorption by this gas is negligible [Hoff and Millán, 1981]. The sampling strategy was similar to that which we used in previous studies of volcanic plumes [e.g., Stith et al., 1978; Radke. 1982; Hobbs et al., 1982; Casadevall et al., 1981]. Measurements in quiescent plumes were made in and beneath the vertically stabilized portion of the plume, with the aircraft penetrating the plume normal to its axis (i.e., normal to the mean direction of the wind) at distances of ~7 to 176 km from the mountain. In the large eruption of January 8 we focused primarily on the remote sensing of the emissions with the lidar, since in-plume flying was potentially hazardous.

Mass fluxes of particles, water vapor, $SO_4^=$, CO_2, HCl, SO_2, and NO_x were calculated from the cross-sectional areas of the plumes determined from the lidar, the in situ measurements of the concentrations of these constituents, and average wind speeds. Wind speeds were obtained from the National Weather Service rawinsondes launched from Anchorage, King Salmon, and Kodiak, Alaska, and from a VLF Omega navigational system aboard the research aircraft. In situ measurements of constituents in the plumes were matched for various ranges downwind of the volcano with corresponding lidar (and hence plume cross-sectional area) measurements by flying the aircraft beneath the plume.

Mass concentrations of particles were determined from particle sizing instruments aboard the aircraft assuming spherical particles with a density of 2×10^3 kg m^{-3} [Hobbs et al., 1982] for all of the samples except those taken during the large eruption of January 8 when a density of 3×10^3 kg m^{-3} was used [Stith et al., 1978]. Masses of particles <5 μm diameter were measured directly by weighing 37-mm-diameter Teflon filters that had been exposed to the volcanic plumes. Aerosols were collected for sulfate analysis on 47-mm Teflon filters followed by LiOH impregnated backup filters for HCl collection [Kritz and Rancher, 1980]. Particles were also collected on 0.2-μm Nucleopore filters for scanning electron microscope analysis. In addition, during the June 11 flight, several $AgNO_3$ impregnated filters were exposed for H_2S measurements [Saltzman and Cooper, 1988].

Water vapor in and out of the plumes from the volcano was determined from a high resolution (20 Hz) infrared absolute humidity sensor (Ophir Model 2000). These measurements showed great variability in water vapor content, with standard deviations equal to the mean value in some cases.

All of the measurements listed above, with the exception of water vapor, were obtained by collecting a "grab bag" sample of the plume air [Hegg et al., 1987] and then supplying this sample to various instruments aboard the aircraft. The time to fill the "grab bag" ranged from ~5–15 sec. Since the time taken to penetrate the plume was generally longer than this, the sample was often representative of only a portion of the plume. Therefore to obtain a better estimate of the fluxes of materials in the plume, the various measured parameters were scaled to the Aitken nucleus concentrations, which were measured continuously in the free airstream and provided a good indication of the spatial structure of the plume along the flight path. Thus the cross-sectional area of the plume determined from the lidar, the structure of the plume as indicated by the Aitken nucleus measurements, and the species concentration measurements were all used in determining the flux of species in the plume.

A brief description of the University of Washington's Convair C-131A research aircraft facility, and listing of the instruments aboard, is given in Appendix A. A summary of the methods used to calibrate the instruments and to ensure reliable measurements is given in Appendix B.

Lidar Observations

The dual wavelength lidar proved to be excellent for determining the locations of the particulate emissions from Mount Redoubt. Also, the lidar was of great value in providing measurements of vertical cross-sectional areas of the volcanic plume, which were used in postanalysis to determine the fluxes of particles and gases from the volcano.

Satellite imagery detected the paroxysmal eruption on January 8 as a roughly oval cloud drifting downwind of Mount Redoubt, but it provided very little detailed structural information and no information on the depth of the plume. The airborne lidar, on the other hand, showed the volcanic plume in great detail.

Shown in Plate 1a is a depiction in false color imagery of a vertical cross section of the lidar backscattering measurements from the volcanic plume about 3 hours after the paroxysmal eruption on January 8 and at a distance of ~130 km from the volcano. The plume is seen to be about 50 km wide and 2 km thick. Ash veils, produced by the fallout of ash particles from the plume, can also be seen. At higher levels the lidar detected another layer of volcanic materials (8.6 km msl) near and beyond the edges of the main volcanic plume. However, due to attenuation of the lidar beam, the upper layer was not detected above the denser central regions of the lower volcanic plume.

The intraeruptive emissions observed from January 4–7 were nearly continuous but very variable in intensity and showed considerable complexity in their cross sections. For example, Plate 1b shows a plume cross section, as detected by the lidar, at ~1432 Alaskan local time (ALT) on January 4 at ~18 km from Mount Redoubt. It can be seen that the plume was separating into two portions. About 20 min later the aircraft passed under the plume at a range of ~50 km from Mount Redoubt (Plate 1c). The plume was now considerably more extended laterally, and the breakup into two portions was nearly complete. This example (and many others not shown here) reveals that it cannot be assumed that volcanic plumes are simply cone shaped, with an approximately bell- (or Gaussian) shaped variation in density across their widths.

Another complex plume cross section is shown in Plate 1d. Here frequent steam explosions were superimposed on more continuous emissions that lofted some ash particles and submicron-sized aerosol to ~4.5 km msl. Visual observations, even from the aircraft and by experienced observers, failed to reveal the complexity of the volcanic plumes that the lidar depicted so well.

Lidar appears to be capable of detecting volcanic particulates even under some adverse meteorological conditions. For example, on January 11, 1990, ice crystal aggregates were falling from a deep cloud system over the Cook Inlet. However, the volcanic plume from Mount Redoubt was still detectable at $\lambda = 0.534$ μm in the real-time lidar display (Plate 1e), and with some additional computer processing (Plate 1f) the plume is readily apparent. However, an intervening water cloud a few hundred meters deep would certainly attenuate the lidar beam to the point that a volcanic plume on the other side of the cloud would not be detectable.

Fluxes of Particles and Gases

Our estimates of the mass fluxes of various constituents from Mount Redoubt are summarized in Table 1. Water vapor was the dominant constituent (by mass) in the Redoubt emissions, followed by CO_2 and SO_2. For the intraeruptive emissions the water vapor flux averaged ~4300 ± 3600 kg s^{-1}, CO_2 averaged ~480 ± 600 kg s^{-1}, and SO_2 averaged ~70 ± 60 kg s^{-1}. There was essentially no CO in the plume. Mass fluxes for $SO_4^=$, HCl and NO_x were all <3 kg s^{-1} and frequently <1 kg s^{-1}. The mass fluxes of particles for the intraeruptive emissions averaged 3 kg s^{-1}. From March 20–24, 1990, we measured SO_2 from Mount Redoubt using the correlation spectrometer mounted on a light aircraft; the mass fluxes of SO_2 derived from these measurements ranged from ~18–75 kg s^{-1}.

The SO_2 fluxes that we measured during the intraeruptive emissions from Mount Redoubt are similar to those that we measured in intraeruptive emissions from the neighboring Mount St. Augustine volcano in 1976, where the average value was ~100 kg s^{-1} [Stith et al., 1978]. Measurements at St. Augustine in 1986 by Rose et al. [1988] showed an SO_2 flux of 24,000 tons day^{-1} (278 kg s^{-1}) during the eruptive phase but only 380 tons day^{-1} (4.4 kg s^{-1}) 3 months later. Similar results were found by Greenland et al. [1985] at Kilauea, Hawaii, at various stages in its eruption, and by Rose et al. [1986] at the White Island volcano in New Zealand. The average SO_2 flux that we measured for the intraeruptive emissions from Mount St. Helens, Washington, in 1980–1981 was substantially lower at ~2 kg s^{-1} [Hobbs et al., 1982; Casadevall et al., 1983] and similar to Mount Erebus, Antarctica, which was 1–3 kg s^{-1} [Radke, 1982; Rose et al., 1985; Chuan et al., 1986].

The average water vapor flux (~3000 kg s^{-1}) that we measured in the intraeruptive emissions from St. Augustine [Stith et al., 1978] was similar to Mount Redoubt (~4300 kg s^{-1}). Mount St. Helens produced greater quantities of water vapor (~100,000 kg s^{-1}) during its intraeruptive emissions [Hobbs et al., 1982]. The average mass fluxes of particles <48 μm in diameter in the intraeruptive emissions from these volcanoes varied from ~3 kg s^{-1} for Mount Redoubt, to ~80 kg s^{-1} for Mount St. Helens, to ~330 kg s^{-1} for St. Augustine.

Measurements made in the large eruption of Mount Redoubt on January 8, 1990, were limited to particles. The fluxes of particles with diameters <48 μm, derived from these measurements, ranged from ~7000–12000 kg s^{-1} and averaged ~10^4 kg s^{-1}. For comparison the particle flux that we derived for the paroxysmal eruption of Mount St. Helens on May 18, 1980, was ~6 x 10^4 kg s^{-1}, and for St. Augustine on February 8, 1976, it was ~6 x 10^5 kg s^{-1}. However, it should be noted that due to differences in sampling locations with respect to the plumes, rapid variabilities in volcanic emissions, and other factors, comparisons of measurements between volcanoes should be treated with some caution. This is especially true for measurements made in large eruptions, which may be hampered by potentially hazardous flying conditions.

Measurements of particles and trace gases made in the posteruptive emissions from Mount Redoubt on June 11, 1990, show a general decrease in the volcano's activity compared to January 1990 (Table 1). The average mass flux of particles with diameters <48 μm measured in June 1990 was <0.1 kg s^{-1} compared to average values as high as 8 kg s^{-1} in January. The average CO_2 flux was ~50 kg s^{-1} in June compared to average values as high as 1714 kg s^{-1} in January. However, the average water vapor flux measured in June (~6400 kg s^{-1}) was somewhat higher than the average value measured in January (~4300 kg s^{-1}). Measurements of SO_2 fluxes from the volcano on June 11, 1990, obtained from the correlation spectrometer aboard the Convair C-131A aircraft, averaged ~23 kg s^{-1}. SO_2 fluxes derived from the airborne in situ and lidar measurements ranged from 2–5 kg s^{-1}, but due to a leak in the sample line feeding the in situ SO_2 instrument, the latter values were certainly underestimates. The H_2S flux, measured by the impregnated filter technique on June 11, was 0.09 kg s^{-1}.

The particle fluxes measured in the posteruptive emission from Mount Redoubt on June 11 were comparable to those measured by us in the posteruptive emissions from Mount St.

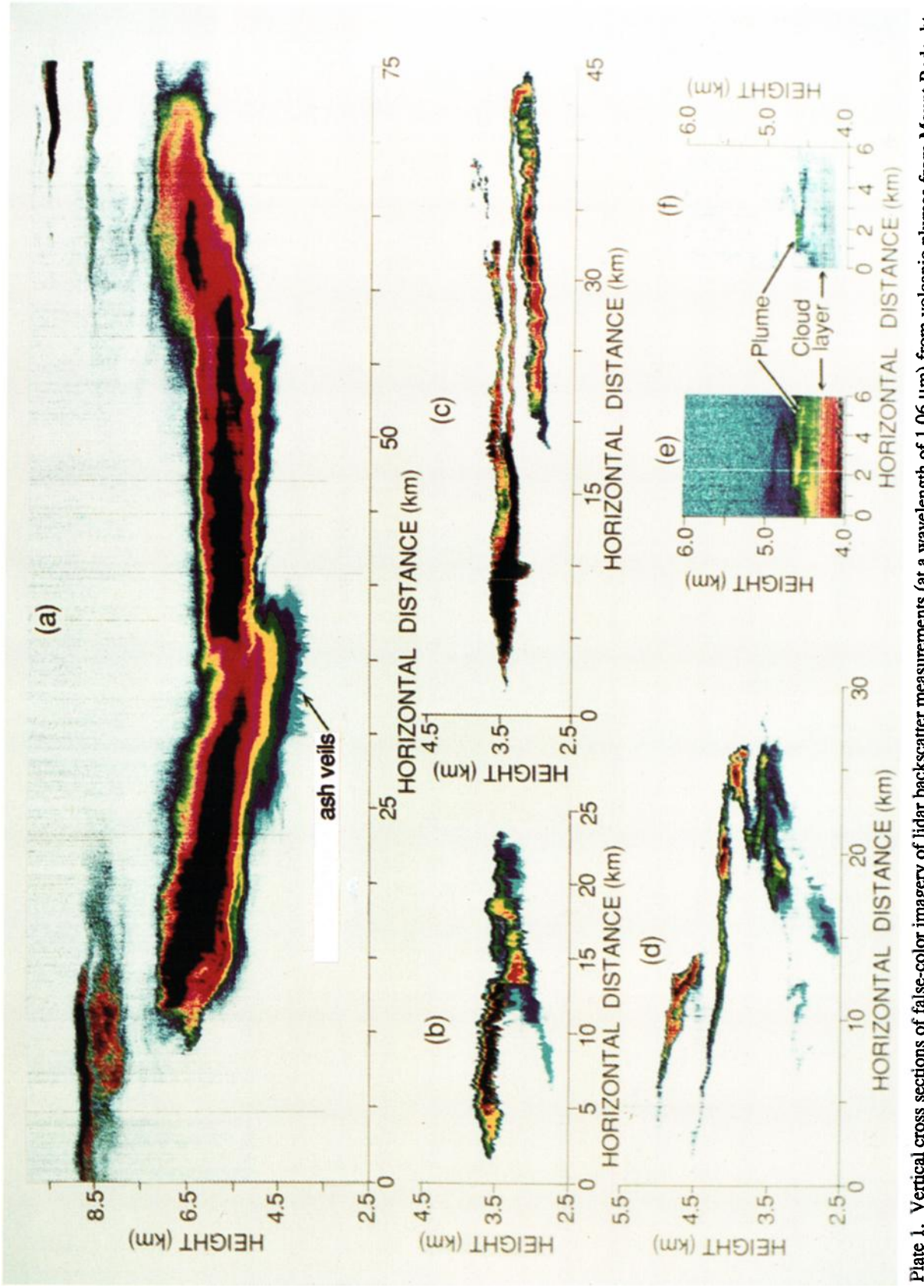

Plate 1. Vertical cross sections of false-color imagery of lidar backscatter measurements (at a wavelength of 1.06 μm) from volcanic plumes from Mount Redoubt. All examples are at $\lambda = 1.06$ μm except (e) and (f) which are at $\lambda = 0.53$ μm. The false colors have been processed to remove the effects of range. Black/red indicates the largest backscatter values and blue/white the least. The same color may represent different backscatter values for the six cross sections shown. (a) January 8, 1990, at 1246:05–1257:03 Alaskan local time (ALT) and ~130 km downwind. (b) January 4, 1990, at 1430:10–1433:45 ALT and ~18 km downwind. (c) January 4, 1990, at 1450:10–1457:45 ALT and ~50 km downwind. (d) January 6, 1990, at 1119:30–1124:35 ALT and ~56 km downwind. (e) January 11, 1990, at 1307:30–1309:00 ALT and ~172 km downwind. (f) Same as (e) with additional computer processing.

TABLE 1. Estimates of the Mass Fluxes (in kg s^{-1}) of Various Constituents From the Redoubt Volcano

Date, Time[a]	Distance From Volcano, km	Particles <48 μm in Diameter[b]	Particles <5 μm in Diameter	Sulfate	Water Vapor[c]	CO_2[c]	SO_2	HCl	NO_x[d]
Jan. 4, 1990					Intraeruptive Emissions				
1413	18	3							
1421	18		4			280	101		0.8
1508	28			0.2	5787	127	75	2.4	0.8
1521	24	7			9349				
1548	28	1	2		5342	189	72		0.6
		(4)	(3)	(0.2)	(6826)	(199)	(83)	(2.4)	(0.7)
Jan. 5, 1990									
1243	22	13	6		11315	420	128		2.7
1321	32	7	5		3853	365	135		1.4
1428	65		3		9506	127	80		0.5
1510	56			2.0	15010	330	226	1.5	2.4
1515	61	2			7505				
		(7)	(5)	(2.0)	(9438)	(310)	(142)	(1.5)	(1.8)
Jan. 6, 1990									
1205	80	1	8		0	1057	107		2
1233	80	5	7		8765	617	166		2
1237	78	8			14024				
		(5)	(8)		(7597)	(837)	(137)		(2.0)
Jan. 7, 1990									
1348	32		1		184	117	45		0.8
1355	32	1			184				
1410	37	0.5			368	52			0.02
1506	22	2		0.1	737	127	42	<DL	0.5
		(1.1)	(1)	(0.1)	(368)	(98)	(43)	(<DL)	(0.4)
Jan. 8, 1990					Paroxysmal Emissions				
1231	~130	7,472							
1234	~130	12,554							
		(10,013)							
Jan. 11, 1990					Intraeruptive Emissions				
1308	167		0.9			34	1.5		<0.1
1314	176	0.6			163				
		(0.6)	(0.9)		(163)	(34)	(1.5)		(<0.1)
Jan. 12, 1990									
1504	28	0.6			378				
1509	18	0.6	2.3	0.06	567	277	20	<DL	0.3
1516	18	1.5			0				
1525	37			0.06	2142	214	24	<DL	0.4
1533	37				3063				
1557	22	0.4			7180				
1602	20	0.8			8125				
1612	18		0.4		4913	98	22	<DL	0.3
		(0.8)	(1.4)	(<0.1)	(3296)	(197)	(22)	(<DL)	(0.3)
June 11, 1990					Posteruptive Emissions				
1140	9	0.08			7826	48	5[e]		
1207	7	0.06			4906	59	2[e]		
		(0.07)			(6366)	(54)	(3.4)[e]		

Average values are in parentheses.
DL is detection limit.
[a]Alaskan local time in hours and minutes.
[b]Particle density assumed to be $2x10^3$ kg m^{-3} except for the first two samples on January 8, when the density was assumed to be $3x10^3$ kg m^{-3}.
[c]After subtracting ambient values.
[d]NO_x flux based on an estimate of 98% NO_2 and 2% NO.
[e]Underestimates due to leak in sample line.

Helens (<1 kg s^{-1}) [Hobbs et al., 1982] and from three Central American volcanoes [Casadevall et al., 1984], but they were lower than those measured in St. Augustine in 1976 (~30 kg s^{-1}) [Stith et al., 1978]. The posteruptive SO_2 fluxes from Mount Redoubt were similar to those measured from Mount St. Helens (~10 kg s^{-1} in 1980 and ~0.2 kg s^{-1} in 1981) and from St. Augustine in 1976 (~20 kg s^{-1}). These values are also similar to the SO_2 fluxes measured from the quiescent Arenal volcano, Costa Rica, (~2 kg s^{-1}), the Colima volcano, Mexico (~4 kg s^{-1}), and the Poas volcano, Costa Rica, (~9 kg s^{-1}) [Casadevall et al., 1984], and Kilauea (~5 kg s^{-1}) [Chartier et al., 1988]. These comprise a fairly small fraction of the estimated global volcanic emissions of ~600 kg s^{-1} [Stoiber et al., 1987].

The fluxes of all the measured constituents from Mount Redoubt varied considerably during the course of a flight and from one day to another, reflecting both the nonsteady state nature of the volcanic activity (Figure 1) and differences in position of the aircraft with respect to the plume. The mass fluxes of particles measured in the large eruption of Mount Redoubt on January 8 (~7000–12,000 kg s^{-1}) were by far the largest that we measured from Mount Redoubt (and are off the scale of Figure 1). With a few exceptions, higher mass fluxes of particles from Mount Redoubt were accompanied

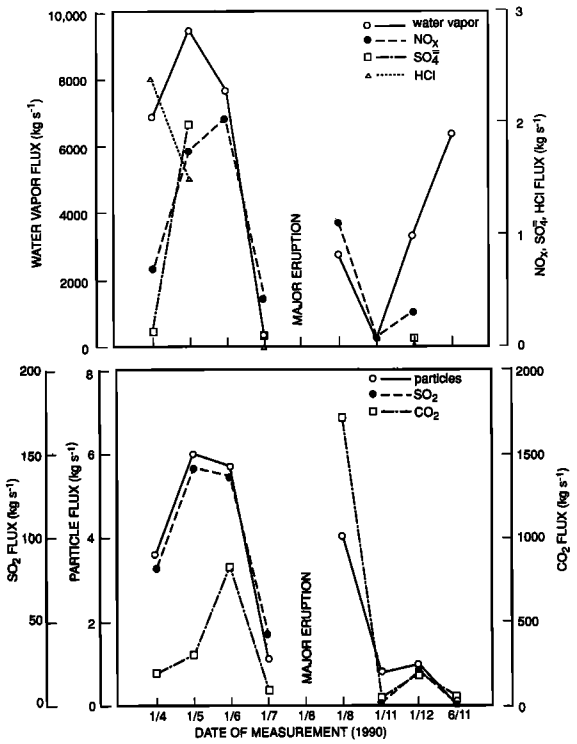

Fig. 1. Average mass fluxes of various constituents measured in plumes from the Redoubt Volcano. The particle fluxes are for particles <48 μm diameter. Estimates of the mass flux of particles < 48 μm in diameter in the paroxysmal eruption on January 8 ranged from ~7000–12,000 kg s^{-1}.

by higher mass fluxes of the gases we measured. A similar pattern was observed following the May 18 and May 25, 1980, eruptions of Mount St. Helens, Washington [Hobbs et al., 1982], and the February 8 and February 13, 1976, eruptions of St. Augustine, Alaska [Stith et al., 1978]. However, our observations of Mount St. Helens and St. Augustine indicated that this trend did not continue during the posteruptive phase. For these two volcanic eruptions the mass fluxes of water vapor and SO_2 in the posteruptive phases were highly variable, but these variations were not matched by corresponding changes in particle fluxes. We have not sampled the volcanic emissions from Mount Redoubt sufficiently during its posteruptive phase to establish any pattern.

Particle Measurements

As noted in Appendix B, measurements of the size specra of aerosol involves bringing air samples into the Convair aircraft, which introduces the potential for particle losses in the sampling system. Comparisons with ground-based measurements have shown that such losses are negligible for submicrometer-sized particles. However, for particles with radii in excess of about 5 μm the losses can be substantial. Hence the concentrations given below for particles with radius greater than about 5 μm must be viewed as minimum concentrations; the actual concentrations in the air may be as much as a factor of 3 greater than those given.

Four examples of particle size distributions measured in the emissions from Mount Redoubt are shown in Figure 2: two for intraeruptive emissions (A and D) and two measured in the emissions (B and C) from the large eruption on January 8. All four particle number distributions contain a nucleation mode (<0.1 μm diameter) and an accumulation mode (~0.1–1.0 μm diameter), although these modes are most prominent in intraeruptive emissions.

The two intraeruptive spectra are very similar in shape, except that the intraeruptive emissions (D) sampled after the January 8 eruption are substantially depleted in accumulation mode particles. Both of the intraeruptive spectra have peak number modes at ~0.1 μm and ~0.8 μm diameters. The number mode at ~0.1 μm, seen in spectra A and D, was probably the product of a condensation process (primarily H_2SO_4 in equilibrium with H_2O), which may have been produced by homogeneous nucleation. SEM-EDAX analysis showed that a significant fraction of the particle mode at ~0.8 μm consisted of silicate fragments.

Although the duration of the large eruption on January 8 was only about 15 min [Brantley, 1990], the emissions produced an easily recognizable eruptive cloud for at least 7 hours (when darkness fell). Measurements made in this eruptive cloud ~2 1/2 hours after the start of the main

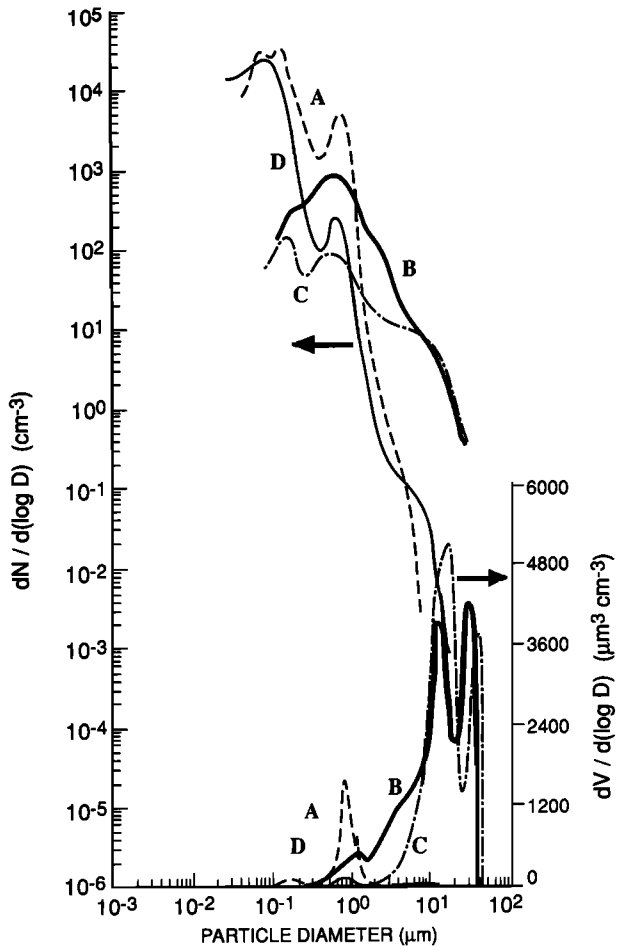

Fig. 2. Examples of particle number and volume size distributions in the emissions from Mount Redoubt: A, January 5, 1990, intraeruptive emission, 3.8 km msl, 22 km downwind; B, January 8, 1990, paroxysmal emission, 4.0 km msl, ~130 km downwind and ~2 1/2 hours after the main eruption; C, January 8, 1990, aged paroxysmal emission, 2.6 km msl, ~170 km downwind and ~7 hours after the main eruption; D, January 12, 1990, intraeruptive emission, 2.7 km msl, 20 km downwind.

eruption (spectrum B in Figure 2) contained mostly accumulation mode and large (>1.0 μm diameter) particles and comparatively few nucleation mode particles. Particle spectrum C, sampled ~7 hours after the eruption, shows the effects of aging on particle sizes in the paroxysmal emissions. In the ~4 1/2 separating spectrum B and C, particles of all sizes decreased in concentrations. However, nucleation mode particles were relatively more prominent in the older sample C.

Virtually all of the particle volume (or mass) in the intraeruptive emissions was contained in accumulation mode particles with diameters of ~0.8 μm (see volume plots in Figure 2). Most of the particle mass in the eruption cloud on January 8 was composed of giant sized (10–100 μm diameter) particles predominantly of diameters ~10 μm and ~30 μm (see double peak in spectrum B volume plot, Figure 2). These large particles continued to make up a large fraction of the particle mass in the aged paroxysmal emissions (spectrum C in Figure 2).

The particle number distributions described above for the emissions of Mount Redoubt on January 8 show some marked differences from those measured in the emissions from Mount St. Helens [Hobbs et al., 1982] and St. Augustine [Stith et al., 1978] (see Figure 3). The emissions from St. Augustine (spectrum X in Figure 3) and St. Helens (spectrum Y in Figure 3) contained large concentrations of nucleation mode particles, whereas accumulation mode particles dominated the number distributions in the eruptive emission from Mount Redoubt (spectrum B in Figure 3). In addition, the eruptive clouds of both Mount St. Helens and St. Augustine produced two peaks in the number distributions between 0.3 and 2 μm diameter, which were not measured in the emissions from Mount Redoubt. It is interesting to note that the aged emissions from Mount Redoubt (spectrum C in Figure 3) show a second particle mode that looks very similar to that measured in the eruptive emissions from St. Helens and St. Augustine. All three volcanoes contained giant sized particles in their paroxysmal emissions. Also, they all produced significant emissions of millimeter-sized debris, but these had extremely short residence times in the atmosphere. In the eruptive emissions from Mount St. Helens and St. Augustine the particle volume (or mass) distributions were dominated by the giant sized particles; however, there is a suggestion of a mode in the volume distributions at ~8–10 μm diameter. The masses of the particles in the eruptive emissions from Mount Redoubt was composed primarily of ~10-μm and 30-μm-diameter-sized particles. Emissions from all three volcanoes produced a less significant volume mode centered at ~1–2 μm diameter.

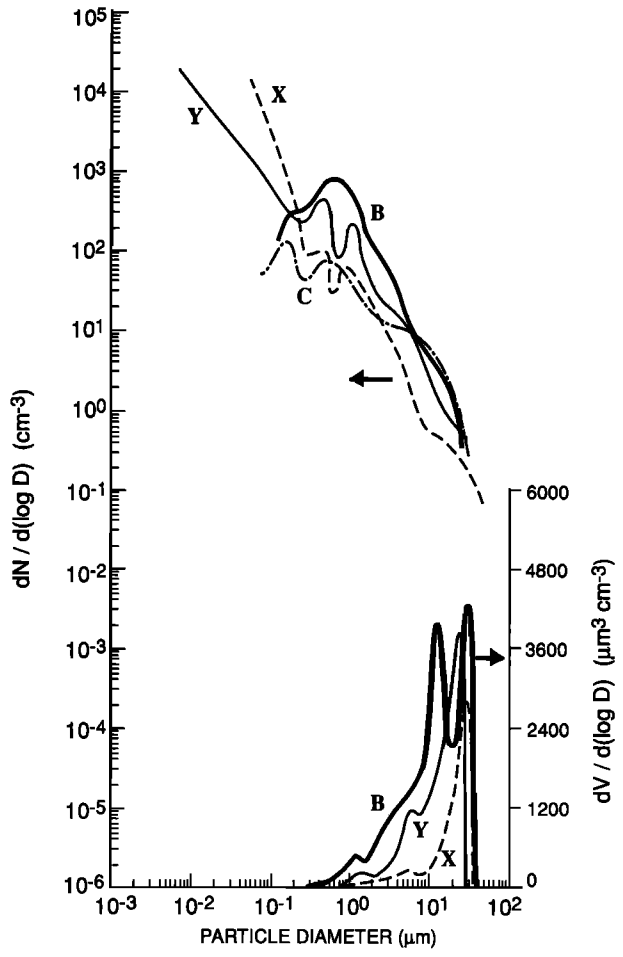

Fig. 3. Particle number and volume distributions in paroxysmal emissions from several volcanoes. B and C are as in Figure 2 (for clarity the volume distribution for C is not repeated); X, St. Augustine, February 8, 1976, ~55 km range; and Y, Mount St. Helens, May 18, 1980, ~9 km range.

The mass concentrations of particles and gases that we measured in the intraeruptive and posteruptive emissions from Mount Redoubt are listed in Table 2. The average value of the total mass concentrations of particles with diameters <5 μm was ~120 ± 60 μg m^{-3} (see Table 2). This agrees rather well with the mass concentration of particles < 3 μm diameter calculated from the particle volume distribution assuming a particle density of 2 x 10^3 kg m^{-3}, which for the same samples averaged 135 ± 190 μg m^{-3}. Only about 20% (usually much less) of the particle mass in the plumes consisted of sulfate, which was present in concentrations ranging from 1.5 to 53 μg m^{-3}, with a mean value of 6 ± 20 μg m^{-3} (Table 2). Hence most of the fine (< 3 μm diameter) particle mass in the emissions from Mount Redoubt probably consisted of mineral materials. The two flights on which the highest mass concentrations of particles with diameters less than 0.3 μm were measured (January 5 and January 7) also had the highest sulfate concentrations, indicating that the strikingly prominent nucleation mode near 0.1 μm diameter consisted of H_2SO_4, which was produced either in the volcanic throat or by gas-to-particle conversion of SO_2 in the plume. A similarly predominant nucleation mode was observed in the plume from Mount Erebus [Radke, 1982].

Further insight into the nature of the submicron particles was gained from scanning electron microscope analysis of individual particles collected in the intraeruptive emissions from Mount Redoubt. This showed particles devoid of any sulfuric acid coating (Figure 4a). Even the submicrometer particles showed little evidence of sulfur (Figure 4b); they usually had elemental compositions similar to the larger ash particles. These submicrometer particles were probably fragments of larger particles produced by a sand blasting process of the type that produces submicron-sized dust particles in high winds in the Sahara Desert [Gomes et al., 1990]. Volcanic particles from Mount Erebus in Antarctica are also ash particles devoid of sulfuric acid coating [Chuan et al., 1986], as were particles from the 1986 eruption of St. Augustine [Rose et al., 1988]. This contrasts dramatically with the emissions from three Central American volcanoes in which even relatively large ash particles were heavily coated

TABLE 2. Mass Concentrations of Particles and Gases Measured in the Intraeruptive and Posteruptive Emissions From Mount Redoubt

Date, Time[a]	Location	Mass Concentration of <5 μm Diameter Particles From 37 mm Filters, μg m^{-3}	Calculated Masses From Particle Sizing Instruments			$SO_4^=$, μg m^{-3}	HCl, μg m^{-3}	SO_2, μg m^{-3}	NO_x, μg m^{-3}	Sulfur in $SO_4^=$ / Sulfur in SO_2, %
			d<0.3 μm, μg m^{-3}	d=0.3 μm – 3 μm, μg m^{-3}	d<48 μm, μg m^{-3}					
Jan. 4, 1990										
1413	Plume	–	13.6	141	157	–	–	–	–	–
1421	Plume	193	–	–	–	–	–	4527	33.2	–
1439	Under plume	34	0.1	0.2	1.2	–	–	605	4.9	–
1508	Plume	–	–	–	–	4.5	66	2064	18.7	0.15
1548	Plume	122	5.9	75	81	–	–	3807	35.4	–
Jan. 5, 1990										
1243	Plume	287	45	667	718	–	–	>5670	116.3	–
1321	Plume	159	30	220	251	–	–	5127	49.6	–
1428	Plume	120	18	207	226			3224	21.8	–
1510	Plume	–	43	293	342	53	39	>5670	59.7	>0.62
Jan. 6, 1990										
1204	Plume	118	1.5	14	16	–	–	1555	33.6	–
1232	Plume	97	9.8	60	70	–	–	2424	26.7	–
1325	Plume	–	–	–	–	1.5	18	1270	1.1	0.08
Jan. 7, 1990										
1348	Plume	89	–	–	–	–	–	3584	67.2	–
1355	Plume	–	14	71	99	–	–	–	–	–
1441	Background (haze)	–	1.7	1.2	3.4	0.8	<DL	<DL	<DL	–
1506		–	21	145	181	15	<DL	>5670	59.2	>0.18
Jan. 11, 1990										
1214	Plume in cloud	89	4.9	41	60	–	–	957	17.8	–
1308	Plume in cloud	70	4.9	42	58	–	–	124	3.9	–
Jan. 12, 1990										
1509	Plume	119	4.4	23	34	2.2	<DL	1098	18.2	0.13
1525	Plume	–	6.8	32	695[b]	3.5	<DL	1281	19.2	0.18
1541	Background	53	–	–	–	0.1	<DL	<DL	3.1	–
1602	Plume	–	11.8	28	54	–	–	–	–	–
1612	Plume	37	–	–	–	–	–	1715	25.7	–

Dash (–) is no data.
DC is detection limit.
[a]Alaskan local time in hours and minutes.
[b]Sample contains ash particles.

with sulfuric acid [Cadle et al., 1979; Casadevall et al., 1984]. It is likely that in the cold wintertime conditions of Alaska, relatively little of the SO_2 emitted is photochemically oxidized to H_2SO_4, which would then condense onto the ash particles. Indeed, comparisons of the mass concentrations of sulfate and SO_2 in the intraeruptive emissions from Mount Redoubt show that only a fraction of 1% of the SO_2 had oxidized to sulfate during the first few hours following emissions from the caldera (Table 2). This contrasts with the much lower SO_2 to $SO_4^=$ ratios found in Central American volcanic plumes by Cadle et al. [1979] and Lazrus et al. [1979], where several percent of the SO_2 was converted to sulfate.

Summary and Conclusions

In this paper we have described airborne in situ and remote sensing measurements of the volcanic emissions from Mount Redoubt during the period January 4–12, 1990, and on June 11, 1990. We have characterized the emissions in terms of particle and gas fluxes and particle size distributions, concentrations, and compositions. We have also provided examples of the horizontal and vertical structures of the ash-bearing volcanic plumes as revealed by an airborne lidar.

The volcanic emissions during the eruptive period consisted mainly of water vapor (~4300 kg s^{-1}), followed by CO_2 (~480 kg s^{-1}) and SO_2 (~70 kg s^{-1}). In the intraeruptive emissions the fluxes of $SO_4^=$, HCl, NO_x, and particles were on average $\lesssim$3 kg s^{-1}; less than 20% of the particle mass consisted of sulfates. The sulfate appears confined to the 0.1 μm mode aerosol. Very little of the SO_2 (~0.1%) was oxidized to sulfate, and the SEM-EDAX analysis showed that nearly all of the particles lacked a sulfuric acid coating. This is in sharp contrast to volcanic particles observed in more temperate locations where photochemistry is much more active [Casadevall et al., 1984].

Measurements in one of Mount Redoubt's major explosive eruptions in 1990 (January 8) showed that the fluxes of particles <48 μm in diameter were ~10^4 kg s^{-1}. This large flux was due to large number of particles >1 μm diameter, with a peak mass concentration at $\gtrsim$10 μm diameter. Few particles <1 μm diameter were found in the paroxysmal emissions compared to the intraeruptive emissions.

The posteruptive emissions from Mount Redoubt had smaller particle mass (<0.1 kg s^{-1}) and CO_2 fluxes (~50 kg s^{-1}) than the intraeruptive emissions (~3 kg s^{-1} and ~480 kg s^{-1}, respectively). Also, correlation spectrometer measure-

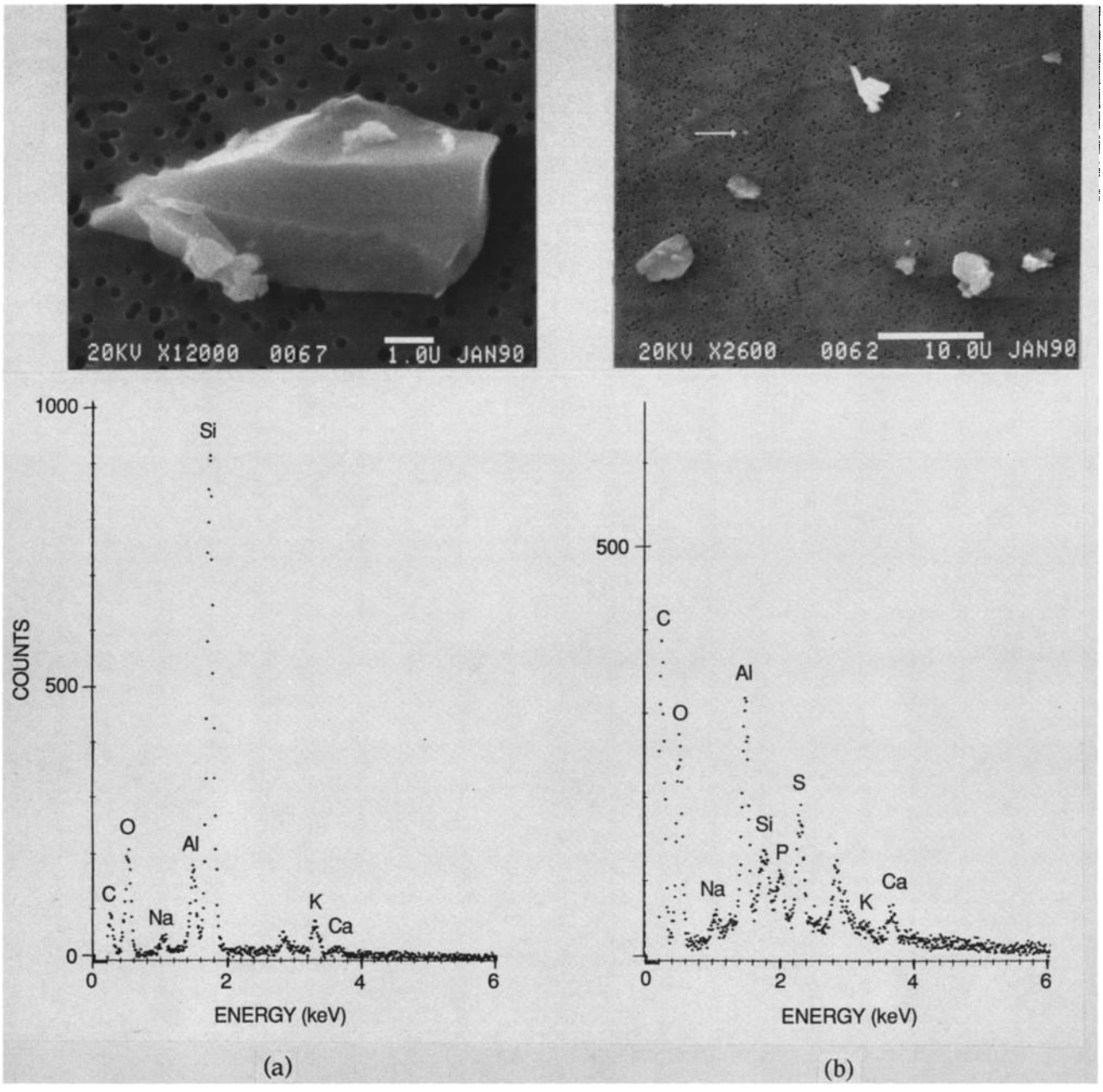

Fig. 4. a) Typical large (~10 μm) ash particle and corresponding elemental analysis showing pure mineral composition with no sulfuric acid coating. b) Several large and small ash particles. (The white line at the bottom represents 10 μm.) The elemental analysis is for one of the submicron particles (arrow), which shows a trace of sulfur and no sulfuric acid coating. Most other submicron particles contained only mineral elements with no evidence of sulfur.

ments showed a decrease in SO_2 flux (to ~23 kg s^{-1}). The water vapor flux remained a large component of the posteruptive emissions (~6400 kg s^{-1}).

This study has demonstrated the great utility of lidar for determining the location and structure of volcanic plumes containing ash. Also, estimates of mass fluxes were significantly improved by the use of the lidar to determine cross-sectional areas of the plumes. It must be noted however that our success in the use of the lidar was due in part to the clear weather that predominated during our studies. In the presence of weather clouds the utility of lidar for detecting volcanic plumes may be significantly reduced.

Appendix A: University of Washington's Convair C-131A Research Aircraft

General Description of Airborne Facilities

The Convair C-131A is a twin-engine, propeller-driven aircraft that is large enough to carry a large instrumentation payload plus a crew of up to eight persons. The layout of the work stations and major instrumentation units on the aircraft is shown in Figure A.1. (See Table A.1 for key.)

Details on the instrumentation presently aboard the aircraft are given in Table A.2, where they are grouped under

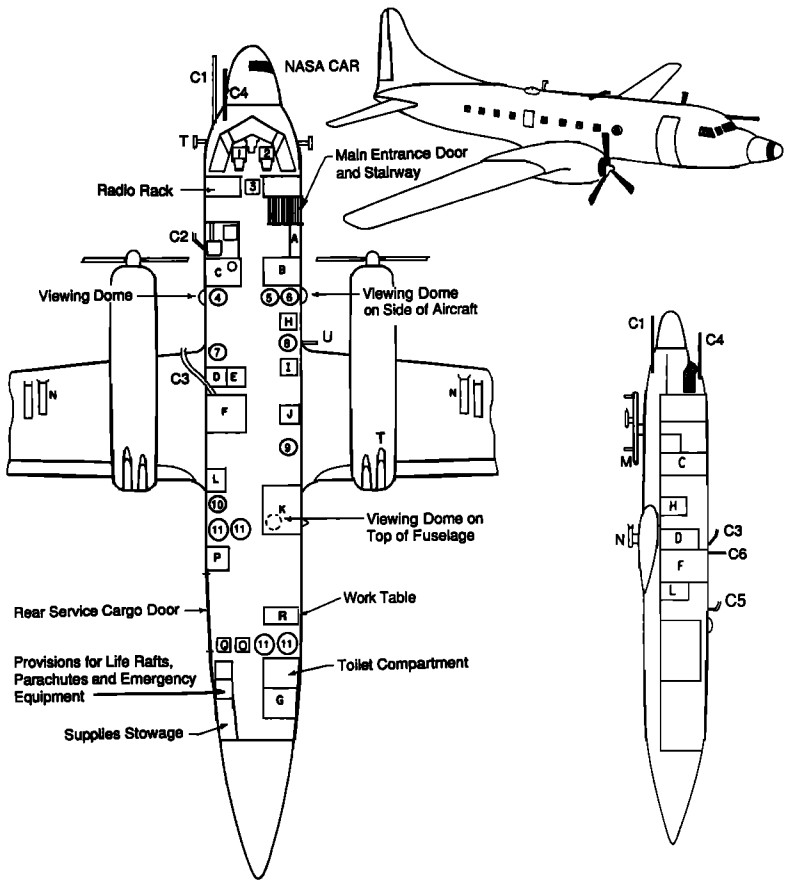

Fig. A.1. Layout of work stations and major research instrumentation units aboard the University of Washington's Convair C-131A research aircraft. (See Table A.1 for key to numbers and letters.)

TABLE A.1. Key to Numbers and Letters in Figure A-1

Number, Letter	Description
1	Pilot
2	Copilot
3	Flight scientist or meteorologist
4	Aerosol scientist
5	Flight scientist or meteorologist
6	Flight scientist or meteorologist
7	Chemist
8	Flight engineer
9	Cloud absorption radiometer (CAR) operator
10	Cloud condensation nucleus (CCN) counter operator
11	Takeoff and landing stations for science crew
A	Inverters and power distribution
B	Scientific situation display including digital and graphical monitors, analog and digital hard copies, radio, and telecommunications
C	Primary aerosol characterization system
C1	Inlet supplies the grab sampler
C2	Inlet supplies the heated plenum and high volume sample ports
C3	Inlet supplies the 1.5 m^3 bag sampler and the trace gas detection system
C4	Inlet for 7-m-long light extinction and light scattering cells
C5	Inlet for counterflow virtual impactor
C6	Inlet for cloud water sampler

TABLE A.1. (Continued)

Number, Letter	Description
D	Trace gas system for DMS, NO, NO_2, HNO_3, PAN, SO_2, O_3, CO, and CO_2
E	Cloud water and wet chemistry system for hydrometeor inorganic and some organic ions and aqueous H_2O_2
F	Enclosed 1.5-m^3 bag sampler and aerosol filter system
G	Vacuum pump cabinet
H	Data computer and recording system
I	Controls for meteorological sensors
J	Cloud absorption radiometer controls and data recorder
K	Sensor for DMS and hemispheric viewing dome
L	Cloud condensation nucleus spectrometer
M	Pod (located on aircraft belly under position 3) liquid water sensors (Johnson-Williams and King); UW ice particle counter and PMS FSSP probe
N	Under wing mounts for 1- and 2-D PMS cloud and precipitation probes
O	Visible and UV net radiometers on the top and bottom of fuselage; sea surface temperature sensor on bottom of fuselage
P	Lidar data system and counterflow virtual impactor controls
Q	Nd-YAG lidar
R	35 GHz (λ = 0.86 cm) radar
S	Antennas for 35 GHz radar (upward and downward looking on top and bottom of wing)
T	Ophir IR optical hygrometer

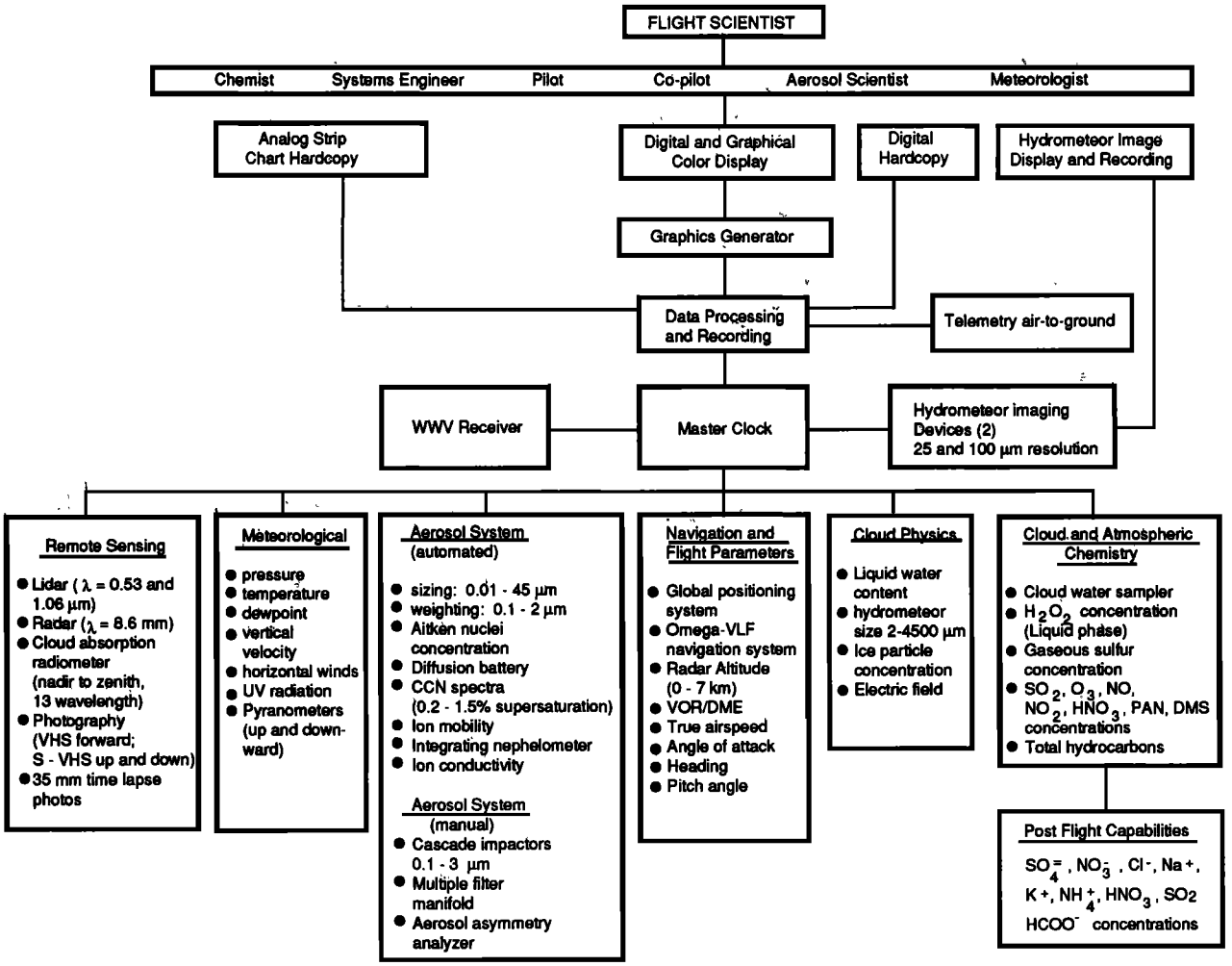

Fig. A.2. Scientific crew, measuring systems, and data display and recording systems aboard the University of Washington's Convair C-131A research aircraft.

the following headings: navigational and flight characteristics, general meteorological, cloud physics, aerosol, cloud and atmospheric chemistry, remote sensing, and data processing and display. The interrelationships among the scientific crew, the various measurement systems, and the data display and recording systems are shown schematically in Figure A.2.

Data Recording and Data Display

Data from the various instruments aboard the aircraft are digitized and distributed to both a microcomputer for on-board display and an independent digital tape cartridge recording system for postflight analysis. The flight scientists, systems engineer, cloud and aerosol scientist, and atmospheric chemist stations each have terminals and color graphics displays to access data from the computer via a multiuser operating system (see Figure A.2). Software is available to display up to 20 measured parameters, as well as particle and droplet spectra, aircraft position plots, histograms of selected parameters, and radar/lidar reflectivity profiles. Fast data-rate instrumentation (such as the lidar, 35 GHz radar, and cloud absorption radiometer) employs separate high density magnetic tape recording systems. Time synchronization is assured by the use of a clock signal common to all the measuring systems.

Appendix B: Calibration of Instruments

The University of Washington's Convair C-131A research aircraft carries a wide variety of instruments to measure various meteorological, chemical, aerosol, and radiative parameters (see Appendix A). We give here a brief summary of some of the calibration procedures used for the various groups of instruments.

TABLE A.2. Instruments Aboard the University of Washington's Aircraft

Parameter	Instrument Type	Manufacturer	Range (and error)
	Navigational and Flight Characteristics		
Latitude and longitude, ground speed, and horizontal winds	VLF Omega navigator	Litton LTN-3000	0 to 300 m s^{-1} (± 1 m s^{-1} ground speed and ± 1° drift angle)
True airspeed	Variable capacitance	Rosemount Model 831 BA	0 to 250 m s^{-1} (< 0.2%)
Heading	Gyrocompass	King KCS-55A	0 to 360° (± 0.5°)
Pressure altitude	Variable capacitance	Rosemount Model 830 BA	150 to 1100 mbar (< 0.2%)
Altitude above terrain	Radar altimeter	AN/APN22	0 to 6 km (< 5%)
Aircraft position and course plotter	Derived from VLF Omega	In-house	180 km (1 km)
Angle of attack	Potentiometer	Rosemount Model 861	± 23° (< 0.5°)
Rate of climb	Variometer	Ball Engineering	± 12 m s^{-1}
	General Meteorological		
Total air temperature	Platinum wire resistance	Rosemount Model 102CY2CG + 414 L Bridge	-60 to 40°C (< 0.1°C)
Static air temperature	Reverse-flow thermometer	In-house	-60 to 40°C (< 0.5°C)
Electric field intensity	Cylindrical field mill	Modified MRI Model 611	0 to 50 kV (< 1 kV)
Dew point	Dew condensation	Cambridge Systems Model TH73-244	-40 to 40°C (< 1°C)
Absolute humidity	IR optical hygrometer	Ophir Corporation Model IR-2000	0 to 10 gm^{-3} (~ 5%)
Air turbulence	Differential	Meteorology Research, Inc., Model 1120	0 to 10 $cm^{2/3}$ s^{-1} (< 10%)
Pyranometer(s) (one downward and one upward viewing)	Thermopile	Eppley Laboratories, Inc., Model PSP	0 to 1400 W m^{-2} (~ 1%) 0.3–3 μm

TABLE A.2. (Continued)

Parameter	Instrument Type	Manufacturer	Range (and error)
		General Meteorological (continued)	
Ultraviolet radiation	Barrier-layer photoelectric cell	Eppley Laboratories, Inc. Model 14042	0 - 70 W m^{-2} (< 5%) 0.29–0.385 μm
Photographs	35-mm time-lapse camera	Automax Model GS-2D-111	1 s to 10 min
Video tape	Forward looking video camera plus time code	General Electric	VHS format
Video tape	Upward and downward looking video camera	NEC	S-VHS format
		Cloud Physics	
Liquid water content	Hot wire resistance	Johnson-Williams	0 to 2 and 0 to 6 g m^{-3}
Liquid water content	Hot wire resistance	King/PMS	0 to 5 g m^{-3}
Size spectrum cloud particles	Forward light scattering	Particle Measuring Systems Model FSSP-100X	2 to 47 μm*
Size spectrum cloud particles	Diode occultation	Particle Measuring Systems Model OAP-200X	20 to 300 μm*
Size spectrum of precipitation particles	Diode occultation	Particle Measuring Systems Model OAP-200Y	300 to 4500 μm*
Images of cloud particles	Diode occultation imaging	Particle Measuring Systems Model OAP-2D-C	Resolution 25 μm*
Images of precipitation particles	Diode imaging	Particle Measuring Systems Model OAP-2D-P	Resolution 200 μm*
Ice particle concentrations	Optical polarization technique	In-house	0 to 1000 l-1 detects particles (> 50 μm)*
		Aerosol	
Number concentrations of particles	Light transmission	General Electric Model CNC II and CNC I (in-house modified)	10^2 to 10^6 cm^{-3} (particles > 0.005 μm)*
		Aerosol (continued)	
Cloud condensation nucleus spectrometer	Vertical plate continuous flow	In-house	4 selectable super saturations between 0.2 and 2%
Mass concentration particles	Electrostatic deposition onto matched oscillators	Thermal Systems, Inc., Model 3205	0.1 to 3000 μg m^{-3} (< 0.2 μg m^{-3})
Size spectrum of particles	Electric aerosol analyzer	Thermal Systems, Inc., Model 3030	0.0032 to 1.0 μm*
Size spectrum of particles	90° light scattering	Particle Measuring System (LAS-200)	0.5 to 11 μm*
Size spectrum of particles	Forward light scattering	Royco 245 (in-house modified)	1.5 to 40 μm*
Size spectrum of particles	Diffusion battery with TSI condensation nucleus counter (Model 3760)	Thermal Systems, Inc., Model 3040 with in-house automatic valves and sequencing	0.01 to 0.2 μm*
Size spectrum of particles	35 - 120° light scattering	Particle Measuring Systems Model ASASP-X	0.09 to 3.0 μm (< 0.007 μm)*

TABLE A.2. (Continued)

Parameter	Instrument Type	Manufacturer	Range (and error)
Size spectrum of particles	Forward light scattering	Particle Measuring Systems Model FSSP-100X	2 to 47 μm*
Size-segregated mass concentrations of particles	Cascade Impactor	Sierra Instruments Inc.	0.1 to 3 μm* (6 size fractions)
Light scattering coefficient	Integrating nephelometer	Meteorology Research, Inc., Model 1567 (modified for increased stability and better response time)	1.0×10^{-6} m^{-1} to 2.5×10^{-3} m^{-1}
Light extinction coefficient	Optical extinction cell (2 m path length)	Waggoner Electronics	5×10^{-5} to 10^{-2} m^{-1}
	Cloud and Atmospheric Chemistry		
Cloud water samples	Impaction on slotted rods	In-house modification of ASRC sampler	Bulk cloud water collection efficiency ~ 40% based on analysis of in-house flight data
Cloud droplet nucleus collector	Counterflow virtual impactor	In-house	Drops > 7 μm diameter
	Cloud and Atmospheric Chemistry (continued)		
Particulate sulfur $SO_4^=$, NO_3^-, Cl^-, Na^+, K^+, NH_4^+	Teflon filters CSI and XRF spectroscopy and Dionex ion exchange chromatography	In-house	0.1 to 50 μg m^{-3} (for 500 L air sample)
SO_2	Impregnated filters	In-house	≥ 20 pptv (for 5 m^3 air sample)
SO_2	Pulsed fluorescence	Teco SP43 (modified in-house)	1.0 ppb to 5 ppm
Ozone	Chemiluminescence, C_2H_4	Monitor Labs Model 8410 A	0 to 5 ppm (< 7 ppb)
NO, NO_2, NO_x	Chemiluminescence, O_3	Modified Monitor Labs Model 8840	0 to 5 ppm (~ 1 ppb)
HNO_3	Nylon filters with Teflon prefilter followed by ion chromatography and/or tungstic cid denuder tubes followed by chemiluminescent detection	Dionex/Monitor Labs	Variable
CO	Correlation spectrometer	Teco Model 48	0 - 50 ppm (~ 0.1 ppm)
CO_2	Correlation spectrometer	Customized Teco Model 41H	0 - 1000 ppm (~ 4 ppm)
DMS	Absorption on gold wires, followed by gas chromatography with flame photometric detection	In-house	> 1 pptv (± 10%)
	Remote Sensing		
Absorption and scattering of solar radiation by clouds and aerosols	Scanning cloud absorption radiometer	NASA Goddard/ University of Washington	13 wavelengths between 0.5 and and 2.3 μm

TABLE A.2. (Continued)

Parameter	Instrument Type	Manufacturer	Range (and error)
Radar reflectivity	Pulsed 35 GHz (λ = 0.86 cm) radar	In-house	Upward and downward pointing (600 m to 20 km)
Optical backscatter	Nd-YAG lidar (dual wavelength, polarization diversity)	Georgia Tech and University of Washington	0-15 km (7.5 m resolution)
	Data Processing and Display		
Ground communication	FM transceiver	Motorola	200 km
In-flight data processing	Microcomputer	In-house, based on Motorola MVME-133A technology	–
In flight color graphics	Microcomputer	In-House, based on Motorola MVME-133A technology	–
Recording (digital)	Microcomputer-directed cartridge recorder	In-house, based on 3M technology	–
Recording (digital)	Floppy disk	–	–
Recording (analog voice transcription)	Cassette recorder	Radio Shack	–
Digital printout	Impact printer	Mannesman Tally MT 160	
Analog strip charts	8-channel high-speed ink recorder	Soltec T200-839	–

*All particle sizes refer to maximum particle dimensions.

General Meteorological

Temperature and Dew Point

The probes used to measure air temperature and dew point are designed for aircraft use, and to function properly, they must be ventilated at aircraft velocities. Thus they can be calibrated only in flight or in a wind tunnel.

Our procedure is to periodically calibrate these instruments by flying the aircraft close to a tower where the air temperature and dew point are measured with thermometers and psychometers, the calibration of which can be traced back to National Institute of Standards and Technology (NIST) standards. Also, comparisons are made with concurrent National Weather Service (NWS) radiosonde data.

Wind Direction and Speed

Wind direction and speed are derived using the VLF Omega navigation system aboard the aircraft. The large-scale, average winds are verified on a flight-to-flight basis, by the accuracy of the aircraft navigation. On shorter time scales our measurements of the winds are compared with ground-based and NWS rawinsonde measurements.

Absolute Humidity

Absolute humidity is measured with an infrared (IR) hygrometer. This instrument is calibrated by the manufacturer in an environmental chamber against a chilled-mirror hygrometer, the calibration of which can be traced to a NIST standard.

Cloud Physics

Liquid Water Content

The liquid water meters are periodically calibrated in the high speed icing tunnel of the National Research Council in Ottawa, Canada. The calibrations are generally performed at –15°C. A rotating icing cylinder is the absolute reference method employed at this temperature. Relative calibrations are also performed at temperatures up to 25°C.

Ultraviolet Radiation

The broadband (λ = 0.3–3 μm) pyranometer and the UV (λ = 0.29–0.385 μm) radiometer are calibrated periodically by Eppley Laboratories (the manufacturer) against NIST-

traceable, standard light sources for the specific bandwidths of the instruments.

PMS FSSP-100X

The Particle Measuring Systems (PMS) forward scattering spectrometer probe (FSSP) is regularly checked for proper sizing of particles by dropping glass beads of various known sizes through the laser field of view and determining into which size channels the spectrometer places the resultant signals. The FSSP is a single particle counter; therefore, provided the instrument parameters (e.g., depth of field, strobe rate, boundary trajectory) have been properly set to avoid coincidence counting errors, the concentrations are quite reliable. The performance of the probe is constantly monitored in this regard, and apparent shifts or biases can be identified from time series data analysis. When serious errors occur, the probe is returned to the manufacturer for realignment.

PMS 1-D and 2-D Probes

These probes have their sizing capabilities periodically evaluated by dropping lead shot of various sizes through their fields of view in a manner similar to that used for the calibration of the FSSP. The reliability of the concentration measurements is also assessed in a similar manner to that for the FSSP. As a further check for reliable measurements the cloud liquid water contents, over appropriate droplet size ranges, derived from these probes are compared to the liquid water contents measured by the King and Johnson-Williams meters.

Aerosol Instruments

Inlet Systems

Unlike the cloud physics probes, which measure the hydrometeor size spectrum in situ, the aerosol instruments require air samples to be brought into the aircraft for measurement. This requires the usage of inlet systems, with the consequent possibility of particle losses [Huebert et al., 1990]. Because virtually all such potential losses are due to the velocity of the aircraft (75–86 m s^{-1} for the Convair), we have compared aerosol measurements obtained on the Convair C-131 with those made on the ground and on ships as the aircraft flies close by such sites. These comparisons have shown that submicrometer aerosol particles are measured aboard the aircraft with close to 100% efficiency. However, substantial and variable aerosol losses occur for particles with radii in excess of about 5 μm. For such larger particles the measured concentrations aboard the Convair can be as much as a factor of 2 to 3 below the true concentrations.

Aitken Nucleus Counter

Three Aitken nucleus (or CN) counters are utilized aboard the Convair. These instruments are calibrated against a Gardner counter, which in turn is calibrated against a Pollack counter, which is a primary standard.

Nephelometer

The nephelometer is calibrated by measuring light scattering from standard gases of different composition (e.g., Freon 12, particle-free air) for which the molecular scattering can be derived from Rayleigh theory.

Optical Extinction Cell

The extinction cell is calibrated by generating a "white," or nonabsorbing aerosol and then comparing the measured extinction with the scattering measured by the nephelometer.

Bag Sampling System for Particles

This system consists of the bag (or batch sampler) described by Radke [1983] and four discrete particle sizing instruments: a Royco 245 particle counter that covers the size range 1.5 to 40 μm, a PMS LAS-200 that measures particles between 0.5 and 11 μm, a PMS ASASP-X that measures particles between 0.09 and 3 μm, and a TSI electrostatic aerosol analyzer (EAA) that covers particle sizes from ~0.003 to 1.0 μm. Occasionally, a TSI diffusion battery is also used. The FSSP-100X can measure unactivated particles in the size range from 2–47 μm, provided the concentrations are not too high.

The ASASP-X and the EAA are calibrated by generating salt particles with bubblers or nebulizers, using an electrostatic classified to render the particles monodispersed in various sizes, measuring the concentrations with a CN counter, and feeding the monodispersed aerosols to the analyzers. For larger particles, measured by the LAS-200 and the Royco 245, glass beads of various sizes are used for calibration.

CCN Counter

The cloud condensation nucleus (CCN) counter is calibrated for concentrations by comparison with particle counts measured by a CN counter on a monodisperse aerosol generated by an electrostatic classifier. The supersaturations of each chamber are checked by generating salt particles of various sizes and determining the size at which counts are first recorded in a particular chamber. The supersaturation in the chamber can then be determined from the calculated activation supersaturation of the particle size first recorded by the chamber.

Cloud and Atmospheric Chemistry

CO and CO_2 IR Spectrometers

Both of these devices are calibrated by measurement of traceable span gases of various concentrations. This is generally done on each flight.

O_3 Analyzer

This chemiluminescent detector is calibrated against an ozone generator which, in turn, is calibrated against a NIST-certified UV absorption cell.

SO_2 Analyzer

The pulsed-fluorescence SO_2 analyzer is calibrated against an SO_2 permeation tube and NIST-certified span gases used in a dynamic dilution system.

NO_x Analyzer

The two-channel (NO and NO_x) NO_x analyzer is calibrated against two standards. The NO channel is calibrated against NIST-certified span gases in a dynamic dilution system. The NO_x channel is calibrated against an NO_2 permeation tube and a NIST-certified span gas.

DMS Tubes

The gold tube scrubbers used to collect dimethyl sulfide (DMS) have been assessed for sample breakthrough and collection efficiency by laboratory tests. Also, several field intercomparisons have been undertaken and one recent laboratory audit conducted by NIST. The DMS technique as a whole was found to reproduce NIST standards to within a few percent.

Filter Packs

The filter pack measurements of particulate ionic species and gaseous SO_2 are evaluated by determination of sampling efficiencies and recovery efficiencies in the laboratory. Field intercomparison with other techniques (for SO_2) have also been carried out. Recently, the SO_2 filter has been tested against a NIST standard with excellent agreement being obtained.

Remote Sensing

Lidar

The dual wavelength lidar, used for measurements of optical backscatter, has only been qualitatively evaluated. The procedure for this is described by Brock et al. [1990].

Scanning Cloud Absorption

This instrument, built and maintained by Goddard Space Flight Center, is periodically calibrated at Goddard against spectrally fine light sources of known intensity at the various discrete wavelength channels of the instrument. Before and after each field deployment a relative calibration is performed by measuring the instrument's response to a broadband light source with well-characterized and constant intensity. This permits assessment of possible degradation of the silicon detectors in the instrument.

Acknowledgements. The rapid deployment to Anchorage and the success of our field study was greatly aided by Senator T. Stevens and aide D. Gibson, D. Hodgkins (FAA), J. Fletcher and B. Hicks (NOAA/ERL), J. Evans and M. Stone (MIT Lincoln Laboratories), B. Goldenburg, H. Hassel, and J. Kemper (NOAA/NWS/Anchorage), and D. Keil (FAA/Anchorage). E. Saltzman (University of Miami) provided filters and analysis of H_2S. We extend our sincere thanks to each of these individuals. We are also grateful to many others, too numerous to mention by name, who helped us in this work. This work was sponsored by MIT Lincoln Laboratories and the Federal Aviation Administration (contract BX 3703) and the National Oceanic and Atmospheric Administration (contracts NA85ABH0031 and NA90RAH0073). The views expressed are those of the authors and do not reflect the official policy or position of the U.S. Government.

References

Alaska Volcano Observatory Staff, The 1989–1990 eruption of Redoubt Volcano, Eos, 71, 265–275, 1990.

Brantley, S. R. (Ed), The eruption of Redoubt Volcano, Alaska, December 14, 1989 – August 31, 1990, U.S. Geol. Surv. Circ. 1061, 33 pp., 1990.

Brock, C. B., L. F. Radke, and P. V. Hobbs, Sulfur in particles in Arctic hazes derived from airborne in situ and lidar measurements, J. Geophys. Res., 95, 22,369–22,387, 1990.

Cadle, R. D., A. L. Lazrus, B. J. Huebert, L. E. Heidt, W. I. Rose, D. C. Woods, R. L.Chuan, R. E. Stoiber, D. B. Smith, and R. A. Zielinski, Atmospheric implications of studies of Central American volcanic eruption clouds, J. Geophys. Res., 84, 6961–6968, 1979.

Casadevall, T. J., D. A. Johnston, D. A. Harris, W. I. Rose, Jr., L. L. Malinconcio, Jr., R. E. Stoiber, T. J. Bornhorst, S. N. Williams, L. Woodruff, and J. M. Thompson, SO_2 emission rates at Mount St. Helens from March 29 through December, 1980, in The 1980 Eruptions of Mount St. Helens, edited by P. W. Lipman and D. R. Mullineaux, U.S. Geol. Surv. Prof. Pap. 1250, 193–200, 1981.

Casadevall, T. J., W. Rose, T. Gerlach, L. P. Greenland, J. Ewert, R. Wunderman, and R. Symonds, Gas emissions and the eruptions of Mt. St. Helens through 1982, Science, 221, 1383–1385, 1983.

Casadevall, T. J., W. I. Rose, Jr., W. H. Fuller, W. H. Hunt, M. A. Hart, J. L. Moyers, D. C. Woods, R. L. Chaun, and J. P. Friend, Sulfur dioxide and particles in quiescent volcanic plumes from Poas, Arenal, and Colima volcanoes, Costa Rica and Mexico, J. Geophys. Res., 89, 9633–9641, 1984.

Chartier, T. A., W. I. Rose, and J. B. Stokes, Detailed record of SO_2 emissions from Pu'u O'o between episodes 33 and 34 of the 1983–86 IRZ eruption, Kilauea, Hawaii, Bull. Volcanol., 50, 215–228, 1988.

Chuan, R. L., J. Palais, W. I. Rose, and P. R. Kyle, Fluxes, sizes, morphology and compositions of particles in the Mt. Erebus volcanic plume, J. Atmos. Chem., 4, 467–477, 1986.

Gomes, L., G. Bergametti, G. Coude'-Gaussen, and P. Rognon, Submicron desert dusts: A sandblasting process, J. Geophys. Res., 95, 13,927–13,935, 1990.

Greenland, L. P., W. I. Rose, and J. B. Stokes, Air estimate of gas emissions and magmatic gas content from Kilauea Volcano, Geochim. Cosmochim. Acta., 49, 125–129, 1985.

Hegg, D. A., L. F. Radke, P. V. Hobbs, C. A. Brock, and P. J. Riggan, Nitrogen and sulfur emissions from the burning of forest products near large urban areas, J. Geophys. Res., 92, 14,701–14,709, 1987.

Hobbs, P. V., L. F. Radke, and J. L. Stith, Eruptions of the St. Augustine Volcano: Airborne measurements and observations, Science, 195, 871–873, 1977.

Hobbs, P. V., L. F. Radke, M. W. Eltgroth, and D. A. Hegg, Airborne studies of the emissions from the volcanic eruptions of Mount St. Helens, Science, 211, 816–818, 1981.

Hobbs, P. V., J. P. Tuell, D. A. Hegg, L. F. Radke, and M. W. Eltgrowth, Particles and gases in the emissions from the 1980–1981 volcanic eruptions of Mt. St. Helens, J. Geophys. Res., 87, 11,062–11,086, 1982.

Hoff, R. M. and M. M. Millán, Remote SO_2 mass flux measurements using COSPEC, J. Air Pollut. Control Assoc., 31, 381–384, 1981.

Huebert, B. J., G. Lee, and W. L. Warren, Airborne aerosol inlet passing efficiency measurement, J. Geophys. Res., 95, 16,369–16,381, 1990.

Kritz, M. A., and J. Rancher, Circulation of Na, Cl, and Br in the tropical marine atmosphere, J. Geophys. Res., 85, 1633–1639, 1980.

Lazrus, A. L., R. D. Cadle, B. W. Gandrud, J. P. Greenberg, B. J. Huebert, and W. I. Rose, Sulfur and halogen chemistry of the stratosphere and of volcanic

eruption plumes, J. Geophys. Res., 84, 7869–7875, 1979.

Radke, L. F., Sulphur and sulphate from Mt. Erebus, Nature, 299, 710–712, 1982.

Radke, L. F., Preliminary measurements of the size distribution of cloud interstitial aerosol, in Precipitation Scavenging, Dry Deposition, and Resuspension, Vol. I, Precipitation Scavenging, edited by H. R. Pruppacher et al., pp. 71–78, Elsevier Science, New York, 1983.

Radke, L. F., P. V. Hobbs, and J. L. Stith, Airborne measurements of gases and aerosols from volcanic vents in Mt. Baker, Geophys. Res. Lett., 3, 93–96, 1976.

Rose, W. I., R. L. Chuan, and P. R. Kyle, Rate of sulphur dioxide emission from Erebus Volcano, Antarctica, December 1983, Nature, 316, 710–712, 1985.

Rose, W. I., R. L. Chuan, W. F. Giggenbach, P. R. Kyle, and R. B. Symonds, Rates of sulfur dioxide and particle emissions from White Island Volcano, New Zealand, and an estimate of the total flux of major gaseous species, Bull. Volcanol., 48, 181–188, 1986.

Rose, W. I., G. Heiken, K. Wohletz, D. Eppler, S. Barr, T. Miller, R. L. Chuan, and R. B. Symonds, Direct rate measurements of eruption plumes at Augustine Volcano: A problem of scaling and uncontrolled variables, J. Geophys. Res., 93, 4485–4499, 1988.

Saltzman, E. S., and D. J. Cooper, Shipboard measurements of atmospheric dimethylsulfide and hydrogen sulfide in the Caribbean and Gulf of Mexico, J. Atmos. Chem., 7, 191–209, 1988.

Stith, J. L., P. V. Hobbs, and L. F. Radke, Airborne particles and gas measurements in the emissions from six volcanoes, J. Geophys. Res., 83, 4009–4017, 1978.

Stoiber, R. E., S. N. Williams, and B. Huebert, Annual contribution of sulfur dioxide to the atmosphere by volcanoes, J. Volcanol. and Geotherm. Res., 33, 1–8, 1987.

T. J. Casadevall, U.S. Geological Survey, Box 25046 MS 903, Denver, CO 80225.

P.V. Hobbs, J. H. Lyons, R. J. Ferek, and D. J. Coffman, Department of Atmospheric Sciences, University of Washington, AK-40, Seattle, WA 98195.

L. F. Radke, NCAR, Research Aviation Facility, PO Box 3000, Boulder, CO 80307-3000.

(Received December 14, 1990;
revised June 17, 1991;
accepted June 17, 1991.)